Global root zone storage capacity from satellite-based evaporation

L. Wang-Erlandsson[1,2], W. G. M. Bastiaanssen[2,3], H. Gao[2,4], J. Jägermeyr[5], G. B. Senay[6], A. I. J. M. van Dijk[7,8], J. P. Guerschman[8], P. W. Keys[1,9], L. J. Gordon[1], and H. H. G. Savenije[2]

[1]Stockholm Resilience Centre, Stockholm University, Stockholm, Sweden
[2]Department of Water Management, Faculty of Civil Engineering and Geosciences, Delft University of Technology, Delft, the Netherlands
[3]UNESCO-IHE Institute for Water Education, Delft, the Netherlands
[4]Global Institute of Sustainability, Arizona State University, Tempe, AZ 85287, USA
[5]Research Domain Earth System Analysis, Potsdam Institute for Climate Impact Research, Potsdam, Germany
[6]US Geological Survey, Earth Resources Observation and Science Centre, North Central Climate Science Centre, Fort Collins, CO, USA
[7]Fenner School of Environment and Society, The Australian National University, Canberra, Australia
[8]CSIRO Land and Water, Canberra, Australia
[9]Department of Atmospheric Science, Colorado State University, Fort Collins, USA

HESSD

doi:10.5194/hess-2015-533

Global root zone storage capacity

L. Wang-Erlandsson et al.

Received: 11 December 2015 – Accepted: 15 December 2015 – Published: 15 January 2016

Correspondence to: L. Wang-Erlandsson (lan.wang@su.se)

Published by Copernicus Publications on behalf of the European Geosciences Union.

Discussion Paper | Discussion Paper | Discussion Paper | Discussion Paper |

HESSD

doi:10.5194/hess-2015-533

Global root zone storage capacity

L. Wang-Erlandsson et al.

Abstract

This study presents an "earth observation-based" method for estimating root zone storage capacity – a critical, yet uncertain parameter in hydrological and land surface modelling. By assuming that vegetation optimises its root zone storage capacity to bridge
5 critical dry periods, we were able to use state-of-the-art satellite-based evaporation data computed with independent energy balance equations to derive gridded root zone storage capacity at global scale. This approach does not require soil or vegetation information, is model-independent, and is in principle scale-independent. In contrast to traditional look-up table approaches, our method captures the variability in root zone
10 storage capacity within land cover types, including in rainforests where direct measurements of root depths otherwise are scarce. Implementing the estimated root zone storage capacity in the global hydrological model STEAM improved evaporation simulation overall, and in particular during the least evaporating months in sub-humid to humid regions with moderate to high seasonality. We find that evergreen forests are
15 able to create a large storage to buffer for severe droughts (with a return period of 10–20 years), in contrast to short vegetation and crops (which seem to adapt to a drought return period of about 2 years). The presented method to estimate root zone storage capacity reduces the dependency on soil and rooting depth data of poor resolution that form a limitation for achieving progress in the global land surface modelling community.

20 ## 1 Introduction

Root zone storage capacity (S_R) determines the maximum amount of soil moisture potentially available for vegetation transpiration, and is critical for correctly simulating recharge and surface runoff (Milly, 1994). Its parameterisation is also important for land-atmosphere interactions, the carbon cycle, and climate modelling (e.g., Bevan
25 et al., 2014; Feddes et al., 2001; Hagemann and Kleidon, 1999; Hallgren and Pitman, 2000; Kleidon and Heimann, 1998b, 2000; Lee et al., 2005; Milly and Dunne, 1994;

Discussion Paper | Discussion Paper | Discussion Paper | Discussion Paper |

HESSD

doi:10.5194/hess-2015-533

Global root zone storage capacity

L. Wang-Erlandsson et al.

Zeng et al., 1998), and for irrigation management and crop yield models (e.g., Basti-aanssen et al., 2007; Hoogeveen et al., 2015).

However, root zone storage capacity is very difficult to measure and observe in the field, especially at the larger scales that are relevant for many modelling needs. Root-ing profiles measurements are also scarce, and difficult to generalise since vegetation rooting systems naturally adapt to prevailing climates and soil heterogeneities (e.g., Gentine et al., 2012; Sivandran and Bras, 2013). Even when rooting profiles are avail-able, difficulties arise in translating them to root zone storage capacity, due to variations in root densities, hydrological activity, horizontal spatial heterogeneities, and uncertain-ties in soil profile data including hard pans.

1.1 Background

Broadly six types of approaches to estimate the root zone storage capacity have been suggested or are in use in hydrological and land surface models: the *field observation based approach*, the *look-up table approach*, the *root distribution modelling approach*, the *inverse modelling approach*, the *calibration approach*, and the *mass balance based approach*. These approaches are described below and compared in Table S1. Some of these approaches estimate rooting depth or root profiles, and can be translated to root zone storage capacity through combination with soil plant available water (Sect. 3.2., Eq. 11), even though it is a simplification.

The *field observation based approach* provide estimates of rooting depths based on rooting depth measurements (Doorenbos and Pruitt, 1977; Dunne and Willmott, 1996; Jackson et al., 1996; Schenk and Jackson, 2002; Zeng, 2001) and has the advantage of being constructed from actual observations of vertical rooting distribution (Canadell et al., 1996; Jackson et al., 1996). To scale up rooting depth to the global scale, Schenk and Jackson (2002) used the mean biome rooting depth and Schenk and Jackson (2009) employed an empirical regression model based on reported root profile from literature. However, this method suffers from data scarcity and location bias, and risks unlikely vegetation and soil combinations due to data uncertainty (Feddes et al., 2001).

HESSD

doi:10.5194/hess-2015-533

Global root zone storage capacity

L. Wang-Erlandsson et al.

Moreover, it requires assumptions on water uptake from a certain fraction of the entire observed root profile. Observations show that many woody and herbaceous vegetation species are able to access very deep layers in a variety of soil conditions (Canadell et al., 1996; Stone and Kalisz, 1991), up to 18 m in Amazonian tropical forest (Nepstad

5 et al., 1994), 53 m in the desert of the south-western United States (Phillips, 1963), and 68 m (possibly 140 m) in the central Kalahari dry savannah (Jennings, 1974). However, isolated roots that go very deep does not necessarily mean that vegetation across the landscape can exploit the full soil to that depth.

The *look-up table approach* is used in hydrological and land surface modelling to

10 parametrise root zone storage capacity based on literature values of mean biome rooting depth and soil texture data (e.g., Müller Schmied et al., 2014; Wang-Erlandsson et al., 2014). This approach facilitates land cover change experiments and is grounded in literature, but assumes root zone storage capacity to be a function of merely land cover and soil type, with little consideration for climatic adjustments. This is a major

15 oversight, as plants within the same vegetation type can exhibit a large span of root zone storage capacities in different climates and landscapes by adaptation to environmental conditions (Collins and Bras, 2007; Feldman, 1984; Gentine et al., 2012; Nepstad et al., 1994). Moreover, an incompatibility issue may arise if the literature based rooting depths employs a land cover classification different from that of the land surface

20 model (Zeng, 2001).

The *root distribution modelling approach* predicts vertical rooting depth based on soil, climate, and vegetation data, and assumptions about the soil hydraulic properties and root distribution behaviour. Often, optimal root profiles are derived based on maximised carbon or transpiration gain (e.g., Collins and Bras, 2007; Schwinning and

25 Ehleringer, 2001; van Wijk and Bouten, 2001), sometimes also while being as shallow as possible (e.g., Laio et al., 2006; Schenk, 2008). The optimisation techniques used differ widely, including genetic algorithm (Schwinning and Ehleringer, 2001; van Wijk and Bouten, 2001), physical ecohydrological modelling (Collins and Bras, 2007; Hildebrandt and Eltahir, 2007), simple analytical modelling (Laio et al., 2006), and stochastic

HESSD

doi:10.5194/hess-2015-533

Global root zone storage capacity

L. Wang-Erlandsson et al.

modelling (Schenk, 2008). This approach is powerful for improving the understanding of root profile development and can be useful for land surface models with explicit root distribution description (Smithwick et al., 2014). Nevertheless, further model development is needed to handle all types of environments (e.g., additional routines to handle groundwater uptake, acidic soil horizons, or low soil temperature) (Schenk, 2008).

The *inverse modelling approach* estimate rooting depth using a model to iteratively simulate a variable available from satellite data (e.g., net or gross primary production, absorbed photosynthetically active radiation, or total terrestrial evaporation) with different rooting depth parameterisations (Ichii et al., 2007, 2009; Kleidon and Heimann, 1998a; Kleidon, 2004). This approach has a large spatial coverage while being indirectly observation-based, but is also dependent on soil information as well as the land surface model performance. In addition, the approach tend to overestimate rooting depth in grasslands, shrubs and dry-deciduous forests that survive droughts by senescence (Kleidon and Heimann, 1998a).

The *calibration approach* is widely used in hydrology, whereby a hydrological model is calibrated on the root zone storage capacity, using hydrological records on precipitation, runoff and evaporation, sometimes in combination with expert knowledge (e.g., Feddes et al., 1993; Fenicia et al., 2008; Jhorar et al., 2004; Winsemius et al., 2009; Gharari et al., 2014). However, the parameters derived are tied to the model used for calibration and are not necessarily comparable to measurable variables in nature, since they tend to compensate for uncertainties in model structure and data. In addition, since discharge is often the only observed variable (or one of only a few), the calibration approach is only suitable for applications at the catchment scale. For global hydrological models, calibration has mostly been performed separately for a selection of large river basins and transferred to other regions using a regionalisation approach (Güntner, 2008; Hanasaki et al., 2008; Hunger and Döll, 2008; Nijssen et al., 2001; Werth and Güntner, 2010; Widén-Nilsson et al., 2007). Nevertheless, challenges remain with discharge data uncertainty and parameter equifinality (Beven, 2006).

HESSD

doi:10.5194/hess-2015-533

Global root zone storage capacity

L. Wang-Erlandsson et al.

Recently, Gao et al. (2014) used a *mass balance approach* – more specifically, the mass curve technique – to estimate the root zone storage capacity at the catchment scale in the US and in Thailand. The underlying assumption is based on the tested hypothesis that plants will not root deeper than necessary (Milly and Dunne, 1994; Milly, 1994; Schenk, 2008). The water demand during the dry season equaled a constant transpiration rate, which was obtained through a water balance approach together with a normalised difference vegetation index (NDVI). Their results suggested that ecosystems develop their root zone storage capacity to deal with droughts with specific return periods, beyond which the costs of carbon allocation to roots are too high from an evolutionary point of view. Yet another mass balance approach was applied by de Boer-Euser et al. (2015) to catchments in New Zealand, using an interception and a root zone storage reservoir to record soil moisture storage deficit from variations in precipitation and transpiration. They derived mean annual transpiration from annual water balances, and seasonality of transpiration was added through estimate of potential transpiration and assumption about vegetation dormancy. The largest storage deficit of individual years were then used to derive catchment representative root zone storage capacity from Gumbel extreme value distribution assuming dry spell return periods of 10 years. These two applications of the mass balance approach have the advantage of being both model-independent and indirectly observation-based. In addition, no land cover or soil information is needed, making the method parsimonious and flexible. Irrigation was, however, not considered and their assumption of ecosystem adaptation does not apply very well to seasonal crops (de Boer-Euser et al., 2015).

In a similar cumulative mass balance approach, van Dijk et al. (2014) combined a satellite evapotranspiration product with monthly precipitation data to estimate a 'mean seasonal storage range' (MSSR) at 250 m resolution across Australia, as one of the inputs into national-scale mapping of groundwater dependent ecosystems (http://www.bom.gov.au/water/groundwater/gde/). MSSR expresses the estimated mean seasonal range in the amount of water stored in all water stores combined (surface, soil and groundwater). A large range was considered likely to indicate a large use of water from

[HESSD](#)

doi:10.5194/hess-2015-533

Global root zone storage capacity

L. Wang-Erlandsson et al.

storage during low rainfall periods from, for example, root water uptake from deeper soil or groundwater stores. Separate mapping of areas subject to irrigation or flood inundation was used to identify areas likely to rely on groundwater. The main conceptual drawback of this method is that the longer-term average seasonal pattern is likely to underestimate rooting depth in general, and even more so in regions without a strong seasonality in rainfall. The method also proved sensitive to any bias in evaporation and rainfall estimates and, in some conditions, simplifying assumptions about runoff and drainage rates (van Dijk et al., 2014).

1.2 Research aims

This study constitute a first attempt to estimate global root zone storage capacity from satellite based evaporation and precipitation data using a mass balance approach, which is possible thanks to recent development, testing and validation of remote sensing evaporation products (e.g., Anderson et al., 2011; Guerschman et al., 2009; Hofste et al., 2014; Hu and Jia, 2015; Mu et al., 2011). Similar to the other mass balance based approaches, we assume that all hydrologically active roots are being used during the driest time and is not deeper than necessary.

Our aims are to: (1) present a method for estimating root zone storage capacity using remote sensing evaporation and precipitation data at global scale that includes the influence of irrigation; (2) evaluate how the new method influences evaporation simulation in a global hydrological model, in comparison to a classical look-up table approach; and (3) investigate the drought return periods different land cover types adjust to. This study, thus, provides an earth observation-based and model-independent estimate of global root zone storage capacity that can be useful in models without the need for root distribution and soil information.

HESSD

doi:10.5194/hess-2015-533

Global root zone storage capacity

L. Wang-Erlandsson et al.

Discussion Paper | Discussion Paper | Discussion Paper | Discussion Paper |

2 Methods

2.1 Estimating root zone storage capacity

The root zone storage capacity S_R is estimated from soil moisture deficit D constructed from time series of water outflow F_{out} and inflow F_{in} from the root zone storage system. The algorithm is conceptually illustrated in Fig. 1.

First, we define the inflows and outflows from the system. The drying F_{out} of the system is the total daily evaporation E:

$$F_{out} = E. \tag{1}$$

Note that the total evaporation E is defined as the sum of transpiration, interception evaporation, soil moisture evaporation and open water evaporation.

The wetting F_{in} of the system is the total daily precipitation P and the evaporation originating from irrigation F_{irr} (i.e., incremental evaporation):

$$F_{in} = P + F_{irr}. \tag{2}$$

We need the term F_{irr} in order to prevent S_R from becoming overestimated in irrigated regions. This is because irrigation is captured in satellite-based evaporation data, but obviously not in precipitation data. Without correction, the irrigation evaporation in the satellite evaporation data would erroneously contribute to accumulation of soil moisture deficit in our computations. In regions (see Appendix A) where the annual accumulated evaporation exceeds annual accumulated precipitation, also the long term average of the difference of $E - (P + F_{irr})$ is added to F_{in} in order to compensate for overestimation of evaporation and underestimation of precipitation.

Second, the difference between inflow and outflow is calculated at the daily scale. The accumulated difference A is represented by the shaded areas in Fig. 1 and can be

HESSD

doi:10.5194/hess-2015-533

Global root zone storage capacity

L. Wang-Erlandsson et al.

defined as

$$\underset{t_n \to t_{n+1}}{A} = \int_{t_n}^{t_{n+1}} F_{\text{out}} - F_{\text{in}} \, dt, \tag{3}$$

where t_n is either the start of the accounting period or a point in time when $F_{\text{out}} = F_{\text{in}}$.
Third, we calculate the moisture deficit D, being the shortage of water from rainfall:

$$D(t_{n+1}) = \max\left(0, D(t_n) + \underset{t_n \to t_{n+1}}{A}\right). \tag{4}$$

The accumulation of D will occur in our algorithm only during periods where $F_{\text{out}} > F_{\text{in}}$, and reductions of D will occur when $F_{\text{out}} < F_{\text{in}}$. However, in order to take into account surface runoff, D never becomes negative (see Fig. 1 at t_2). In this way, for every hydrological year, one maximum accumulated moisture deficit can be determined, representing the largest annual drought. In addition, D is reset to zero by the end of a three years period in a few grid cells where D accumulation persist for three years or more. Such increases are likely the effect of lateral supply of water, or reflect erroneous combinations of P and E. The resetting of this limited number of pixels does not affect the outcome of this study in any measureable way. A long time series of these maximum annual values creates the opportunity to study the return period of the maximum moisture deficits. Extreme values analysis, such as by Gumbel's method (Gumbel, 1935), then yield estimates of extreme moisture deficits with different probabilities of exceedance, see Sect. 2.3.

Finally, in addition to the moisture deficits with a specific probability of exceedance, we also define the largest value of the moisture deficits D over the considered time series of observation, which, assuming the ecosystem was able to deal with this deficit, would be the estimate of the root zone storage capacity (S_R):

$$\underset{t_0 \to t_{\text{end}}}{S_R} = \max(D(t_0), D(t_1), D(t_2), ..., D(t_{\text{end}})). \tag{5}$$

Discussion Paper | Discussion Paper | Discussion Paper | Discussion Paper |

HESSD

doi:10.5194/hess-2015-533

Global root zone storage capacity

L. Wang-Erlandsson et al.

S_R estimate based on an evaporation and precipitation time series would (in the absence of additional water supply) theoretically constitute a *minimum* root zone storage capacity, see Fig. S1 in the Supplement. If the root water uptake by plants does not abstract water until wilting point, the root zone storage may not utilise its full capacity. Note also that the S_R computed is not to be confused with time variable moisture availability. The time-variable water availability can be inferred from hydrological models using S_R as the water holding capacity.

During wet spells, additional fluxes from the soil system include surface runoff and drainage into groundwater. These fluxes only occur after certain levels of saturation have been achieved. Therefore, during prolonged dry spells, which are critical for sizing the root zone storage requirement, these fluxes may be neglected.

2.2 Implementation in a hydrological model

The newly derived root zone storage capacity is used in the global hydrological model STEAM (Wang-Erlandsson et al., 2014) to evaluate its influence on evaporation simulation. STEAM is a process-based model that partitions evaporation into five fluxes (i.e., vegetation interception, floor interception, transpiration, soil moisture evaporation, and open water evaporation). Potential evaporation is computed using the Penman-Monteith equation (Monteith, 1965), surface stomatal resistance is based on the Jarvis-Stewart equation (Stewart, 1988), and phenology is expressed as a function of minimum temperature, soil moisture content and daylight (Jolly et al., 2005). The model operates at 1.5° and 3 hours resolution

In the original version of STEAM, root zone storage capacity is calculated as the product of soil plant available water (depending on soil texture) and rooting depth (depending on land cover type). Here, however, the root zone storage capacity is simply location-bound (depending on climatic variables alone) and no longer considered a land cover and soil based parameter. In the original version of STEAM, the stress func-

HESSD

doi:10.5194/hess-2015-533

Global root zone storage capacity

L. Wang-Erlandsson et al.

tion of soil moisture is:

$$f(\theta) = \frac{(\theta - \theta_{wp})(\theta_{fc} - \theta_{wp} + c)}{(\theta_{fc} - \theta_{wp})(\theta - \theta_{wp} + c)},$$ (6)

where θ is the actual volumetric soil moisture content (dimensionless), θ_{wp} is the volumetric soil moisture content at wilting point, θ_{fc} at field capacity, and c is a soil moisture stress parameter assumed to be 0.07 (Matsumoto et al., 2008; Wang-Erlandsson et al., 2014). To use the root zone storage capacity S_R, we do not account for soil moisture below wilting point and assume $S_R = h(\theta_{fc} - \theta_{wp})$, where h is the rooting depth (m). The reformulated stress function of soil moisture becomes:

$$f(S) = \frac{S(S_R + C)}{S_R(S + C)},$$ (7)

where S is the actual root zone storage (m), and the soil moisture stress parameter C is assumed to be 0.1. This reformulation is possible since the stress function retains its shape. Thus, S_R can in similar ways be implemented in other hydrological models.

To measure improvement, the root mean square error (ε_{RMS}) for simulated evaporation is calculated using the original look-up table based root zone storage capacity $S_{R,STEAM}$ and the newly derived root zone storage capacity S_R respectively. The root mean square error improvement ($\varepsilon_{RMS, imp}$) is positive if the E simulated using S_R is closer to a benchmark evaporation data set than the E simulated using $S_{R,STEAM}$. The equation below shows the $\varepsilon_{RMS,imp}$ of $S_{R,CRU-SM}$, using the remote sensing based ensemble evaporation product E_{SM} as benchmark:

$$\varepsilon_{RMS, imp} = \left[\varepsilon_{RMS}(E_{S_{R,STEAM}}) - \varepsilon_{RMS}(E_{SM})\right] -$$
$$\left[\varepsilon_{RMS}(E_{S_{R,CRU-SM}}) - \varepsilon_{RMS}(E_{SM})\right].$$ (8)

To investigate where the improvements are most significant, improvements in mean annual, mean maximum monthly and mean minimum monthly E is calculated separately.

Discussion Paper | Discussion Paper | Discussion Paper | Discussion Paper |

HESSD

doi:10.5194/hess-2015-533

Global root zone storage capacity

L. Wang-Erlandsson et al.

$\varepsilon_{\text{RMS,imp}}$ by climate are done for bins of precipitation seasonality index and aridity index, both defined in Appendix B. $\varepsilon_{\text{RMS,imp}}$ by land cover types are analysed for grid cells where single land cover occupancy exceeds 90 % in a 1.5° grid cell. ε_{RMS} analyses are carried out on area weighted evaporation values to avoid bias caused by differences in grid cell areas. Results are shown in Sect. 4.3.

2.3 Frequency analysis

We calculate S_{R} for 10 to 11 years (2003–2012 and 2003–2013 respectively, see Sect. 3.1) depending on data availability. However, different ecosystems may adapt their root system depths to different return periods of drought which may or may not correspond to the available data time series length. Thus, we also determine the $S_{\text{R},L\ \text{yrs}}$ for different return periods of drought L (see Sect. 4.4) based on Gumbel's distribution (Gumbel, 1935). The resulting $S_{\text{R},L\ \text{yrs}}$ is a function of the mean and standard deviation of the extremes in the data series:

$$S_{\text{R},L\ \text{yrs}} = \overline{S_{\text{R}}} + \frac{\sigma_{S_{\text{R}}}}{\sigma_n}(y_L - y_n), \tag{9}$$

where y_n is the reduced mean as a function of the number of available years n (y_{10} = 0.4952 and y_{11} = 0.4996), is the reduced standard deviation as a function of n (σ_{10} = 0.9496 and σ_{11} = 0.9676), is the standard deviation of S_{R}, while y_L is the reduced variate of the Gumbel distribution:

$$y_L = -\ln\left(-\ln\left[1 - \frac{1}{L}\right]\right). \tag{10}$$

Discussion Paper | Discussion Paper | Discussion Paper | Discussion Paper |

HESSD

doi:10.5194/hess-2015-533

Global root zone storage capacity

L. Wang-Erlandsson et al.

3 Data

3.1 Evaporation and precipitation input for estimating S_R

We present two S_R datasets, one covering the latitudes 50° N–50° S ($S_{R,CHIRPS-CSM}$), and one with global coverage 80° N–56° S ($S_{R,CRU-SM}$). See Table 1 for an overview of the data input for each S_R dataset.

For the clipped 50° N–50° S $S_{R,CHIRPS-CSM}$ map, we matched the 0.05° USGS Climate Hazards Group InfraRed Precipitation with Stations (CHIRPS) precipitation data (P_{CHIRPS}) (Funk et al., 2014) with the ensemble mean of three satellite-based global scale evaporation datasets (E_{CSM}): the CSIRO MODIS Reflectance Scaling Evapo-Transpiration (CMRSET) v1405 at 0.05° (Guerschman et al., 2009), the Operational Simplified Surface Energy Balance (SSEBop) at 30″ (Senay et al., 2013), and the MODIS evapotranspiration (MOD16) at 0.05° (Mu et al., 2011). These three different evaporation models are all based on MODIS satellite data, but they use different parts of the electro-magnetic spectrum. CMRSET combines a vegetation index, which estimates vegetation photosynthetic activity, and shortwave infrared spectral data to estimate vegetation water content and presence of standing water. SSEBop relies on the thermal infrared data for determination of the latent heat flux and MOD16 on the visible and near-infrared data to account for Leaf Area Index variability. Hence, their input data, model structure and output data are not necessarily similar, which makes them attractive for deriving an ensemble evaporation product. $S_{R,CHIRPS-CSM}$ is based on data covering the years 2003–2012 as CMRSET was not available for 2013.

For the global coverage $S_{R,CRU-SM}$ map, we used the 0.5° Climatic Research Unit Timeseries version 3.22 (CRU TS3.22) precipitation data (P_{CRU}) (Harris et al., 2014) together with the ensemble mean (E_{SM}) of only SSEBop and MOD16, since we found CMRSET to overestimate evaporation at high latitudes, possibly due to the effect of snow cover on estimates. In addition, the irrigation effect was analysed for $S_{R,CRU-SM}$ by including evaporation originating from irrigation water simulated at 0.5° and at the daily scale by the dynamic global vegetation model LPJmL (Jägermeyr et al., 2015).

Discussion Paper | Discussion Paper | Discussion Paper | Discussion Paper |

HESSD

doi:10.5194/hess-2015-533

Global root zone storage capacity

L. Wang-Erlandsson et al.

$S_{R,CRU-SM}$ is computed based on evaporation data covering the years 2003–2013. Irrigation data cover the years 2003–2009 (monthly mean irrigation evaporation were used for years after 2009).

The input precipitation and evaporation data are shown in Figs. 2 and S2 in the Supplement. The mean annual accumulated evaporation of E_{CSM} and E_{SM} is sometimes higher than the mean annual accumulated precipitation P_{CHIRPS} and P_{CRU}, which is discussed in Appendix A.

In addition, ECMWF re-analysis interim (ERA-I) (Dee et al., 2011) daily 0.5° evaporation and precipitation data were used to temporally downscale the monthly evaporation and precipitation data. This allows daily products of evaporation and precipitation, which was necessary in order to incorporate also short drought periods.

3.2 Other data used in analyses

The following datasets were compared with our S_R estimates:

- the estimated 1° rooting depth for 95 % of the roots from Schenk and Jackson (2009);

- the 1° rooting depth estimated by the optimised inverse modelling from Kleidon (2004), (where the minimum rooting depth producing the long-term maximum net primary production is selected as the best estimate);

- the 1° rooting depth estimated by the assimilated inverse modelling from Kleidon (2004), (where the rooting depth that minimises the difference between the modelled and the satellite-derived absorbed photosynthetically active radiation is selected as the best estimate); and

- the root zone storage capacity look-up table based parametrisation used in a global hydrological model, i.e., the Simple Terrestrial Evaporation to Atmosphere Model (STEAM)(Wang-Erlandsson et al., 2014).

Discussion Paper | Discussion Paper | Discussion Paper | Discussion Paper |

HESSD

doi:10.5194/hess-2015-533

Global root zone storage capacity

L. Wang-Erlandsson et al.

In order to enable comparison between rooting depth h and root zone storage capacity S_R, we assumed that the root zone reaches its wilting point and converted between h and S_R using soil properties:

$$S_R = h\theta_{paw} = h\left(\theta_{fc} - \theta_{wp}\right), \tag{11}$$

where θ_{paw} is the maximum plant available soil moisture, θ_{fc} is the volumetric soil moisture content at field capacity and θ_{wp} is the volumetric soil moisture content at wilting point. Soil texture data at $30''$ is taken from the Harmonised World Soil Database (HWSD) (FAO/IIASA/ISRIC/ISSCAS/JRC, 2012), and field capacity and wilting point information is based on the United States Department of Agriculture (USDA) soil classification (Saxton and Rawls, 2006).

To analyse if and how the inferred S_R may improve simulations in a hydrological model, we applied $S_{R,CRU-SM}$ to the evaporation simulation model STEAM. To force STEAM, we used ERA-I evaporation, precipitation, snowfall, snowmelt, temperature at 2 m height, dew point temperature at 2 m height, wind speed in two directions at 10 m height, incoming shortwave radiation, and net long-wave radiation (all at 3 h and 1.5° resolution). To analyse the improvements in simulated evaporation by using $S_{R,CRU-SM}$ as input to STEAM (see Sect. 4.3), we used an aridity index based on precipitation and reference evaporation from CRU TS3.22 (Harris et al., 2014).

For land cover-based analyses, we used the 0.05° Land Cover Type Climate Modeling Grid (CMG) MCD12C1 created from Terra and Aqua Moderate Resolution Imaging Spectroradiometer (MODIS) data (Friedl et al., 2010) for the year 2008, based on the land cover classification according to the International Geosphere – Biosphere Programme (IGBP) (shown in Fig. S3). Land cover fractions are preserved in upscaling to 0.5°. Only 0.5° grid cells containing at least 95 % of a single land cover type are used in the land cover-based analyses (see Sect. 4.2.2) and grid cells containing at least 95 % water are removed from all S_R analyses.

Data with other resolutions than 0.5° have been either upscaled by averaging or downscaled by grid cell values transferring.

Discussion Paper | Discussion Paper | Discussion Paper | Discussion Paper |

HESSD

doi:10.5194/hess-2015-533

Global root zone storage capacity

L. Wang-Erlandsson et al.

Discussion Paper | Discussion Paper | Discussion Paper | Discussion Paper |

HESSD

doi:10.5194/hess-2015-533

Global root zone storage capacity

L. Wang-Erlandsson et al.

4 Results and discussion

4.1 Root zone storage capacity estimates

Figure 3 shows the $S_{R,CHIRPS-CSM}$ (clipped, based on E_{CSM} and P_{CHIRPS}) and $S_{R,CRU-SM}$ (global, based on E_{SM} and P_{CRU}) estimates adjusted for irrigation, (provided in the Supplements as ASCII-files). Independent of the input data used, large root zone storage capacities are observed in the semi-arid Sahel, South American and African savannah, central US, India, parts of Southeast Asia, and northern Australia. The lowest root zone storage capacities are observed in the most arid and barren areas, and in the humid and densely-vegetated tropics. The largest differences between $S_{R,CHIRPS-CSM}$ and $S_{R,CRU-SM}$ are observed over the Amazon, along the Andes, and in Central Asia. Along mountain ridges (for example along the Andes and Himalaya), the S_R estimates are generally larger, possibly due to data uncertainty in these transition regions or evaporation in foothills sustained by lateral water fluxes from the mountains in addition to precipitation.

Notably, Fig. 3 show contrasting root zone storage capacity over the South American and African tropical forests, although they belong to the same ecological class (i.e., evergreen broadleaf forest). This variability is purely due to temporal fluctuations between precipitation and evaporation and is independent of soil properties.

4.2 Comparison to other root zone storage capacity estimates

4.2.1 Geographic comparison

Figure 4 shows root zone storage capacity estimates (directly determined or converted from rooting depth, see Sect. 3.2) from other studies and compares them to $S_{R,CRU-SM}$. The estimates shown are based on: rooting depths containing 95 % of all roots from Schenk and Jackson (2009) ($S_{R,Schenk}$, Fig. 4a), hydrologically active rooting depth from inverse modelling (Kleidon, 2004) using the optimisation ($S_{R,Kleidon,O}$, Fig. 4c) and

Discussion Paper | Discussion Paper | Discussion Paper | Discussion Paper | Discussion Paper

HESSD

doi:10.5194/hess-2015-533

Global root zone storage capacity

L. Wang-Erlandsson et al.

assimilation approach ($S_{R,Kleidon,A}$, Fig. 4e), and from a literature-based look-up table used in the hydrological model STEAM ($S_{R,STEAM}$, Fig. 4g) (Wang-Erlandsson et al., 2014).

When the different datasets are compared to $S_{R,CRU-SM}$ (Fig. 4b, 4d, 4f and 4h), we see both agreements and significant differences. All datasets appear to more or less agree on the approximate range of root zone storage capacity in large parts of the Northern Hemisphere. Around the Equator, all datasets indicate root zone storage capacity to be lower or similar to that of $S_{R,CRU-SM}$ in the tropical forests of the Amazon and the Indonesian islands. In the Congo region and in Central America, $S_{R,Kleidon,O}$ and $S_{R,Kleidon,A}$ are larger than both $S_{R,CRU-SM}$ and the other. In the south temperate zone, $S_{R,CRU-SM}$ appear to correspond to or be lower than the other datasets.

Figure 4 also reveal patterns specific to the different datasets that can be explained by the underlying method used for estimating rooting depth or root zone storage. For example, both $S_{R,Schenk}$ and $S_{R,STEAM}$ contain spuriously large values in the deserts (such as the Sahara and the Gobi) where vegetation is non-existent or extremely sparse. The methods based on satellite data ($S_{R,CRU-SM}$, $S_{R,Kleidon,O}$ and $S_{R,Kleidon,A}$) appear to reflect reality in deserts more accurately. The $S_{R,Kleidon,O}$ presents the largest root zone storage capacities (most pronounced over Africa, India, parts of South America), since this dataset represent an idealised and optimised case. On the contrary, the smallest root zone storage capacities are presented in the Amazon rainforest by $S_{R,Schenk}$. These smaller values could be due to the lack of observations, since $S_{R,Schenk}$ is derived from rooting depth field measurements. But any difference between rooting depth and root zone storage capacity could also be due to discrepancies between actual rooting depth and hydrologically active rooting depth (see also Sect. 3.2). In contrast to the other datasets, $S_{R,STEAM}$ is relatively homogenous and does not contain any large values (basically all < 400 mm) (Fig. 4g). This is natural, since the other datasets are based on more heterogeneous observations, whereas $S_{R,STEAM}$ is based on a homogenous look-up table.

4.2.2 Distribution by land cover type

Figure 5 shows the root zone storage capacity distribution for different land cover types and S_R datasets, ($S_{R,CHIRPS-CSM}$ is not shown since it does not have global coverage). Except for deciduous broadleaf forest, the $S_{R,CRU-SM}$ of forests (Fig. 5a–e) are closer to $S_{R,Kleidon,O}$ and $S_{R,Kleidon,A}$ than to $S_{R,Schenk}$. Interestingly, the range of S_R is large in the evergreen forest types for the "adaptive" estimates ($S_{R,CRU-SM}$, $S_{R,Kleidon,O}$, and $S_{R,Kleidon,A}$), but small for the literature based methods ($S_{R,Schenk}$ and $S_{R,STEAM}$). In open shrubland and grassland (Fig. 5f and i) root zone storage capacities are similar across all estimates, except for the higher $S_{R,STEAM}$. In savannahs, croplands, and natural/vegetation mosaic areas (Fig. 5h, j, k), $S_{R,Kleidon,O}$, and $S_{R,Kleidon,A}$ appear to have higher values than others. In woody savannahs (Fig. 5g), $S_{R,Kleidon,O}$ has a notably large range as well as high mean root zone storage capacity. In barren land (Fig. 5l), $S_{R,Schenk}$ and $S_{R,STEAM}$ are counter-intuitively high.

4.3 Implementation in a hydrological model

We implemented $S_{R,CRU-SM}$, $S_{R,CHIRPS-CSM}$, and $S_{R,STEAM}$ in the hydrological model STEAM (see Sect. 2.2 for methods) in order to analyse how the new root zone storage capacities might improve model performance. This section shows the performance analyses using $S_{R,CRU-SM}$ as input, since it has global coverage. A comparison in E simulation performance between using $S_{R,CHIRPS-CSM}$ and $S_{R,CRU-SM}$ as input to STEAM is shown in Fig. S4 in the Supplement, and discussed in the Supplementary Information.

Figure 6 compares the STEAM-simulated evaporation when using, on the one hand, $S_{R,CRU-SM}$ and, on the other, the look-up table based $S_{R,STEAM}$. The effects on evaporation vary with geography and season. The differences are mainly found in South America outside the tropical wet rainforests, in the Sahel, south of the Congo rainforests and in parts of Southeast Asia. January evaporation simulated with $S_{R,CRU-SM}$ is lower in particularly south of the Sahara, Central America, India, and Southeast Asia, and

Discussion Paper | Discussion Paper | Discussion Paper | Discussion Paper |

HESSD

doi:10.5194/hess-2015-533

Global root zone storage capacity

L. Wang-Erlandsson et al.

higher in Argentina. April evaporation shows only local increases in Central America, Sahel, and Southeast Asia, and minor decreases in South Africa, China, and Argentina. July evaporation shows the largest differences, with both strong evaporation reductions in Brazil, Canada and Europe, and significant increases in the seasonally dry tropical forests in Brazil and in Central Africa. In October, changes in evaporation are again less widespread and mainly affecting South America. It appears that $S_{R,CRU-SM}$ has the greatest potential to influence model simulations for the hot and dry seasons, and for the seasonal tropical forests where the root zone storage capacity varies strongly.

Figure 7 shows the ε_{RMS} improvements of simulated mean annual, mean maximum monthly and mean minimum monthly E sorted by seasonality and aridity, using $S_{R,CRU-SM}$ as input and E_{SM} as benchmark. The analysis reveals that our $S_{R,CRU-SM}$ estimate has the greatest potential to improve model simulations for minimum monthly evaporation. In particular, the improvements become significant with increased seasonality of rainfall, and in subhumid to humid regions, resonating the findings of de Boer-Euser et al. (2015).

4.4 The effect of different drought return periods

Vegetation may adapt to a different time period than the 10–11 years of data that were available for this study. Thus, we normalised S_R using the Gumbel distribution in order to assess the effect of different drought return periods (see Sect. 2.3). Normalised S_R are provided in the Supplements as ASCII-files.

Figure 8 shows the mean latitudinal $S_{R,CHIRPS-CSM,L\ yrs}$ and $S_{R,CRU-SM,L\ yrs}$ for different drought return periods L based on the Gumbel distribution. As may be expected, both $S_{R,CHIRPS-CSM}$ and $S_{R,CRU-SM}$ based on the 10–11 years where data were available correspond most closely to the $S_{R,L\ yrs}$ for $L = 10$ years ($S_{R,10\ yrs}$). $S_{R,L\ yrs}$ always increases with L, but more strongly for small L and less so for large L following the Gumbel distribution. The largest spans are seen in the northern latitudes and around the equator.

Discussion Paper | Discussion Paper | Discussion Paper | Discussion Paper |

HESSD

doi:10.5194/hess-2015-533

Global root zone storage capacity

L. Wang-Erlandsson et al.

Figure 9 shows a comparison of how Gumbel normalised $S_{R,CRU-SM,L\ yrs}$ affect the evaporation simulation ε_{RMS} improvements by land cover type. Interestingly, a drought return period of 2 years ($S_{R,CRU-SM,2\ yrs}$) offers the best evaporation simulation performance in open shrublands, woody savannahs, savannahs, grasslands, croplands and barren lands, whereas $S_{R,CRU-SM,10\ yrs}$ or $S_{R,CRU-SM,20\ yrs}$ are best in evergreen forests and mixed forest. However, performance in deciduous forest is highest with a drought return period of 60 years or more.

A short drought return period of 2 years improves evaporation simulation the most in short vegetation types probably because these land cover types adapt to average years rather than to extreme drought years. In extreme years, they survive by going dormant. Evergreen forests, on the other hand, adapt to 10–20 years of drought return period since they deal with droughts by accessing deeper soil moisture storages and thus invest in root growth (Brunner et al., 2015). The performance increase in deciduous forest by using 60 years of drought return period is more surprising, and we speculate that deciduous forests need a large root zone storage capacity to cater for dry periods during their most active summer months. Alternatively, the larger deciduous forest S_R is simply compensating for thaw or snowmelt processes that the hydrological model does not simulate well. Based on the best performing drought return periods for each land cover types, we created a Gumbel normalised root zone storage capacity map (Fig. S5 in the Supplement), which is shown and analysed (Fig. S6 and Table S3 in the Supplement) in the Supplementary Information. In addition, we also analyse how S_R of different land cover types can be associated with climatic indicators in Appendix B.

4.5 Limitations

Although research indicates that most ecosystem rooting depth are limited by water rather than other resources (Schenk, 2008), other factors may still cause S_R to be larger than what is considered here. A minimum rooting depth of 0.3–0.4 m are for example considered in Schenk and Jackson (2009). Although we are comparing others' rooting depth estimates to $S_{R,CRU-SM}$, they are not directly comparable. Our approach deals

HESSD

doi:10.5194/hess-2015-533

Global root zone storage capacity

L. Wang-Erlandsson et al.

with the accessible water volume in the root zone, which is not always related to root zone depth since the root density can vary over the depth. Our S_R estimates implicitly capture the root density that is active in water uptake.

The $S_{R,CHIRPS-CSM}$ and $S_{R,CRU-SM}$ have been derived using evaporation and precipitation data from recent years (i.e., the 2000s), and should be used with caution if applied to past or future model simulations. Land cover change during the years 2003–2013 have not been taken into account. This has potential impact on the computation of incremental evaporation from irrigated areas with fast changing acreages.

Wetlands and groundwater dependent ecosystems produce incremental evaporation that cannot be ascribed to local rainfall (van Dijk et al., 2014). Bastiaanssen et al. (2014) recently demonstrated for the Nile basin that in some areas, natural withdrawals exceed man-made withdrawals to the irrigation sector. Since satellite evaporation data captures all types of evaporation, and we only corrected for irrigation, natural incremental evaporation sources are implicitly included in $S_{R,CHIRPS-CSM}$ and $S_{R,CRU-SM}$. Thus, our S_R estimates may not strictly represent the root zone storage capacities in regions where water uptake from groundwater is significant, see Fig. A1.

Finally, the quality of the estimated S_R is dependent on the quality of the input evaporation and precipitation data. In particular, the choice of remotely sensed evaporation products influences the resulting S_R more than the choice of precipitation product, because of the generally larger spread in evaporation estimates. Thus, the presented method is preferably applied using an ensemble evaporation product based on reliable datasets identified in comparison and evaluation studies (e.g., Hofste et al., 2014; Hu et al., 2015; Yilmaz et al., 2014; Trambauer et al., 2014). In this study, the largest standard deviations in the ensemble evaporation products are located in central South America, the Sahel, India, and northern Australia (see Fig. 2e, 2f).

Discussion Paper | Discussion Paper | Discussion Paper | Discussion Paper |

HESSD

doi:10.5194/hess-2015-533

Global root zone storage capacity

L. Wang-Erlandsson et al.

5   Summary and conclusion

This study presents a method to estimate root zone storage capacity from remotely sensed evaporation and precipitation data, by assuming that plants do not invest more in their roots than necessary to bridge a dry period. Two global root zone storage estimates ($S_{R,CRU-SM}$ and $S_{R,CHIRPS-CSM}$) are presented based on different precipitation and evaporation datasets, but show in general similar patterns globally. $S_{R,CRU-SM}$ appear to improve mean annual E simulation in STEAM more than $S_{R,CHIRPS-CSM}$, and might be the more accurate product.

Different ecosystems have evolved to survive droughts of different return periods with different strategies. Our analyses showed that whereas long drought return period increased performance for evergreen forests, shorter drought return period increased performance for savannah, crops and other short vegetation types. The best E simulation results were achieved when normalising the S_R estimate using a shorter drought return period (2 years) for short vegetation types, a medium length drought return period (10-20 years) for evergreen and mixed forests, and a long drought return period (60 years) for deciduous forests. This is probably because grasslands survive extreme droughts by going dormant, whereas forests invest in root growth (Brunner et al., 2015). Thus, the root zone storage capacities of short vegetation types seem to adapt to average years, whereas those of forests adapt to extreme years. Normalisation to longer drought return periods should not be done for short-lived annual plants such as two third of the world's croplands (Cox et al., 2006), nor beyond the age of the ecosystem of concern, because vegetation can not be assumed to adapt beyond their age.

The S_R estimates presented here are both globally gridded and observation-based. They have the advantage over the field study based and statistically derived $S_{R,Schenk}$ (Schenk and Jackson, 2009) by being directly based on gridded data and by covering regions where observational studies are limited (e.g., the evergreen broadleaf forests). In comparison to the inverse modelling approaches of Kleidon (2004), the method pre-

Discussion Paper | Discussion Paper | Discussion Paper | Discussion Paper |

HESSD

doi:10.5194/hess-2015-533

Global root zone storage capacity

L. Wang-Erlandsson et al.

sented in this study is independent of model simulations and therefore closer to direct observations.

The new S_R estimates can be used in hydrological and land surface modelling to improve simulation results, particularly in the dry season and in seasonal tropical forests where variations of root zone storage capacity are large. Using the new S_R as input to the hydrological model STEAM improved the evaporation simulation considerably in subhumid to humid regions with high seasonality. In particular, the most significant improvements occurred in the months with the least evaporation. Normalisation of S_R to different drought return periods for different land cover types could further improved evaporation simulation in STEAM, suggesting that Gumbel normalisation is a viable method to optimise the S_R estimates prior to implementation in global hydrological or land surface models.

The presented method is easy to apply and in principle scale-independent. For researchers working at regional or local scales, root zone storage capacities can easily be derived using available evaporation and precipitation data. Moreover, when information on irrigation and groundwater use is available, they can be used to adjust S_R, as was done by for example van Dijk et al. (2014). Satellite-based evaporation datasets are also quickly being developed and improved. New global scale evaporation products such as ALEXI (Atmosphere-Land Exchange Inverse) (Anderson et al., 2011) and ETMonitor (Hu and Jia, 2015) are underway based on 375 and 1000 m pixels. More sophisticated two-layer surface energy balance models also have the capacity to distinguish transpiration from other forms of evaporation. This implies that local root zone storage capacity can be computed, based on transpiration fluxes, which is preferred from a bio-physical point of view (although it would require estimate of interception evaporation to calculate effective precipitation). As new evaporation datasets become available, the S_R estimates can easily be updated. In addition, this method can be used to diagnose and compare different evaporation products, in particular for identifying variations in seasonality. With longer time series of land cover and climate data,

Discussion Paper | Discussion Paper | Discussion Paper | Discussion Paper |

HESSD

doi:10.5194/hess-2015-533

Global root zone storage capacity

L. Wang-Erlandsson et al.

this method can possibly also be used to infer the effect of climate change on root zone storage capacity.

Appendix A: Evaporation exceedance over precipitation

The mean annual accumulated evaporation of E_{CSM} and E_{SM} is sometimes higher than the mean annual accumulated precipitation P_{CHIRPS} and P_{CRU} (see Fig. A1). In these areas, overestimation of S_R may be expected, because it is unlikely that the 10 or 11 year accumulation of E is more than rainfall, except for hydrological situations with lateral inflow through inundation, irrigation or groundwater inflow. The evaporation dataset E_{CSM} exhibits larger and more widely spread exceedance over P_{CHIRPS} in comparison to the $E_{SM} - P_{CRU}$ combination. Most notably, the exceedance is high and potentially spurious in arid and semi-arid zones (e.g., the Sahara, western US, and Central Asia) which suggests that the evaporation from deserts is not accurate. Regions where both the $S_{R,CHIRPS-CSM}$ show high accumulated evaporation exceedance are along the Andes, patches in western US, East Africa, Ivory Coast, Central Asia, Northwest China and spots in Australia. These are essentially irrigated areas, lakes, reservoirs, wetlands and coastal deltas. Possibly, overestimation of S_R can also be caused for example by vegetation tapping into groundwater. Uncertainty in evaporation and precipitation products also propagates to errors in S_R. The uncertainty of evaporation is location specific, (grid cells with a large standard deviation between the individual E products are shown in Fig. 2e and f).

Interestingly, the high evaporation exceedance appears to be much more pronounced during drier years. In Fig. A2, we sort every grid cell by the annual precipitation amount, from dry to wet, and plot the mean latitudinal E exceedance for the regions where the long term accumulated $E - P$ is positive. The figure clearly shows that E exceedance decreases with increase in rainfall, indicating that increased water demand during dry years is satisfied by withdrawing moisture from the soil matrix that

HESSD

doi:10.5194/hess-2015-533

Global root zone storage capacity

L. Wang-Erlandsson et al.

is bounded with more potential (higher pF), or from underlying groundwater through deeply rooting vegetation.

Appendix B: Climatic influence on root zone storage capacity depending on land cover type

B1 Methods and data

We analyse how $S_{R,CRU-SM}$ of different land cover types can be associated with climatic indicators. Stepwise multiple regression method based on the Akaike information criterion (AIC) is used to analyse how these climatic indicators may explain variations in S_R within a land cover type. The climatic indicators used are precipitation seasonality (I_s), aridity (I_a), and interstorm duration (I_{isd}) (as these were found to be important by Gao et al. (2014)):

$$I_S = \frac{1}{\overline{P_a}} \sum_{m=1}^{m=12} \left| \overline{P_m} - \frac{\overline{P_a}}{12} \right|, \text{ and} \tag{B1}$$

$$I_a = \frac{\overline{P_a}}{\overline{E_p}}, \tag{B2}$$

where $\overline{P_m}$ is the mean precipitation of the month, $\overline{P_a}$ is the mean annual precipitation, and $\overline{E_p}$ is the potential evaporation. We defined I_{isd} as the mean continuous number of days per year without precipitation. Interaction effects between the variables are taken into account.

The climate variables interstorm duration, aridity and precipitation seasonality are developed based on monthly 0.5° reference evaporation from CRU TS3.22 (Harris et al., 2014) and monthly 0.5° precipitation for 1982–2009 from the Global Precipi-

HESSD

doi:10.5194/hess-2015-533

Global root zone storage capacity

L. Wang-Erlandsson et al.

Discussion Paper | Discussion Paper | Discussion Paper | Discussion Paper

tation Climatology Centre (GPCC) (Schneider et al., 2011). Here, GPCC data (instead of CRU) are used in order to prevent false correlation with the CRU-based $S_{R,CRU-SM}$.

B2 Results and discussion

We use multiple linear regression to correlate $S_{R,CRU-SM}$ values to climatic indicators, with the aim to investigate how well climate indicators can predict root zone storage capacities in different land cover types. It appears that climate indicators predict root zone storage capacities much better in evergreen forests than in short vegetation types. Figure B1 shows high R^2 in mostly evergreen forests; moderate R^2 in other forest types and croplands; and low R^2 in savannah, shrubland and grassland. This is probably because of their different drought survival strategies. While evergreen forests bridge droughts by water uptake from storage in their root zone, deciduous forests shed their leaves, and short vegetation types such as grassland go dormant and decrease their transpiration to a minimum. The multiple linear regression model for S_R in croplands is moderately explained by climate indicators, potentially due to human management. All climate variables were selected by AIC in the multiple linear regression model (Table B1).

Acknowledgements. This research was supported by funding from the Swedish Research Council (Vetenskapsrådet) and the Swedish Research Council Formas (Forskningsrådet Formas). The global evaporation data sets were made available by the USGS EROS data centre (SSEBop model) and the CSIRO (CMRSET model), and without these data sets, the global upscaling would not have been feasible. We thank USGS FEWS NET (the famine early warning systems network) for making the SSEBop ET data available. We also thank Ruud van der Ent, Ingo Fetzer, Tanja de Boer-Euser, Remko Nijzink, and Tim Hessels for valuable discussions during the manuscript preparation. Finally, we are grateful to Axel Kleidon and Jochen Schenk for sharing and explaining their data.

HESSD

doi:10.5194/hess-2015-533

Global root zone storage capacity

L. Wang-Erlandsson et al.

HESSD

doi:10.5194/hess-2015-533

Global root zone storage capacity

L. Wang-Erlandsson et al.

References

Anderson, M. C., Kustas, W. P., Norman, J. M., Hain, C. R., Mecikalski, J. R., Schultz, L., González-Dugo, M. P., Cammalleri, C., D'Urso, G., Pimstein, A., and Gao, F.: Mapping daily evapotranspiration at field to continental scales using geostationary and polar orbiting satellite imagery, Hydrol. Earth Syst. Sci., 15, 223–239, doi:10.5194/hess-15-223-2011, 2011. 8, 24

Bastiaanssen, W., Allen, R., Droogers, P., D'Urso, G., and Steduto, P.: Twenty-five years modeling irrigated and drained soils: State of the art, Agricult. Water Manage., 92, 111–125, doi:10.1016/j.agwat.2007.05.013, 2007. 4

Bastiaanssen, W., Karimi, P., Rebelo, L.-M., Duan, Z., Senay, G., Muttuwatte, L., and Smakhtin, V.: Earth observation-based assessment of the water production and water consumption of Nile Basin agro-ecosystems, Open Access Remote Sensing special issue on Africa, 2014. 22

Bevan, S. L., Los, S. O., and North, P. R. J.: Response of vegetation to the 2003 European drought was mitigated by height, Biogeosciences, 11, 2897–2908, doi:10.5194/bg-11-2897-2014, 2014. 3

Beven, K.: A manifesto for the equifinality thesis, J. Hydrol., 320, 18–36, doi:10.1016/j.jhydrol.2005.07.007, 2006. 6

Brunner, I., Herzog, C., Dawes, M. A., Arend, M., and Sperisen, C.: How tree roots respond to drought., Front. Plant Sci., 6, 547, doi:10.3389/fpls.2015.00547, 2015. 21, 23

Canadell, J., Jackson, R. B., Ehleringer, J. B., Mooney, H. a., Sala, O. E., and Schulze, E.-D.: Maximum rooting depth of vegetation types at the global scale, Oecologia, 108, 583–595, doi:10.1007/BF00329030, 1996. 4, 5

Collins, D. B. G. and Bras, R. L.: Plant rooting strategies in water-limited ecosystems, Water Resour. Res., 43, W06407, doi:10.1029/2006WR005541, 2007. 5

Cox, T. S., Glover, J. D., Van Tassel, D. L., Cox, C. M., and DeHaan, L. R.: Prospects for developing perennial grain crops, BioScience, 56, 649, doi:10.1641/0006-3568(2006)56[649:PFDPGC]2.0.CO;2, 2006. 23

de Boer-Euser, T., McMillan, H., Hrachowitz, M., Winsemius, H., and Savenije, H.: Influence of soil and climate on root zone storage capacity, Water Resour. Res., in review, 2015. 7, 20

Dee, D., Uppala, S., Simmons, A. J., Berrisford, P., Poli, P., Kobayashi, S., Andrae, U., Balmaseda, M., Balsamo, G., Bauer, P., Bechtold, P., Beljaars, A. C. M., van de Berg, L., Bidlot,

J., Bormann, N., Delsol, C., Dragani, R., Fuentes, M., Geer, A., Haimberger, L., Healy, S., Hersbach, H., Hólm, E., Isaksen, L., Kållberg, P., Köhler, M., Matricardi, M., McNally, A., Monge-Sanz, B., Morcrette, J.-J., Park, B.-K., Peubey, C., de Rosnay, P., Tavolato, C., Thépaut, J.-N., and Vitart, F.: The ERA-Interim reanalysis: configuration and performance of the data assimilation system, Q. J. Roy. Meteor. Soc., 137, 553–597, doi:10.1002/qj.828, 2011. 15

Doorenbos, J. and Pruitt, W. O.: Guidelines for predicting crop water requirement, in: FAO Irrigation and Drainage Paper (FAO), no. 24, p. 144, Rome, 1977. 4

Dunne, K. A. and Willmott, C. J.: Global distribution of plant-extractable water capacity of soil, Int. J. Climatol., 16, 841–859, doi:10.1002/(SICI)1097-0088(199608)16:8<841::AID-JOC60>3.0.CO;2-8, 1996. 4

FAO/IIASA/ISRIC/ISSCAS/JRC: Harmonized World Soil Database (version 1.2), 2012. 16

Feddes, R., Menenti, M., Kabat, P., and Bastiaanssen, W.: Is large-scale inverse modelling of unsaturated flow with areal average evaporation and surface soil moisture as estimated from remote sensing feasible?, J. Hydrol., 143, 125–152, doi:10.1016/0022-1694(93)90092-N, 1993. 6

Feddes, R. A., Hoff, H., Bruen, M., Dawson, T., de Rosnay, P., Dirmeyer, P. A., Jackson, R. B., Kabat, P., Kleidon, A., Lilly, A., and Pitman, A. J.: Modeling root water uptake in hydrological and climate models, Bulletin of the American Meteorological Society, 82, 2797–2809, doi:10.1175/1520-0477(2001)082<2797:MRWUIH>2.3.CO;2, 2001. 3, 4

Feldman, L. J.: Regulation of root development., Annual review of plant physiology, 35, 223–42, doi:10.1146/annurev.pp.35.060184.001255, 1984. 5

Fenicia, F., McDonnell, J. J., and Savenije, H. H. G.: Learning from model improvement: On the contribution of complementary data to process understanding, Water Resour. Res., 44, W06419, doi:10.1029/2007WR006386, 2008. 6

Friedl, M. a., Sulla-Menashe, D., Tan, B., Schneider, A., Ramankutty, N., Sibley, A., and Huang, X.: MODIS Collection 5 global land cover: Algorithm refinements and characterization of new datasets, Remote Sens. Environ., 114, 168–182, doi:10.1016/j.rse.2009.08.016, 2010. 16

Funk, C. C., Peterson, P. J., Landsfeld, M. F., Pedreros, D. H., Verdin, J. P., Rowland, J. D., Romero, B. E., Husak, G. J., Michaelsen, J. C., and Verdin, A. P.: A quasi-global precipitation time series for drought monitoring: U.S. Geological Survey data series 832, Tech. rep., doi:10.3133/ds832, 2014. 14

Gao, H., Hrachowitz, M., Schymanski, S., Fenicia, F., Sriwongsitanon, N., and Savenije, H.: Climate controls how ecosystems size the root zone storage capacity at catchment scale, Geophys. Res. Lett., 41, 7916–7923, doi:10.1002/2014GL061668, 2014. 7, 26

Gentine, P., D'Odorico, P., Lintner, B. R., Sivandran, G., and Salvucci, G.: Interdependence of climate, soil, and vegetation as constrained by the Budyko curve, Geophys. Res. Lett., 39, L19404, doi:10.1029/2012GL053492, 2012. 4, 5

Gharari, S., Hrachowitz, M., Fenicia, F., Gao, H., and Savenije, H. H. G.: Using expert knowledge to increase realism in environmental system models can dramatically reduce the need for calibration, Hydrol. Earth Syst. Sci., 18, 4839–4859, doi:10.5194/hess-18-4839-2014, 2014. 6

Guerschman, J. P., Van Dijk, A. I., Mattersdorf, G., Beringer, J., Hutley, L. B., Leuning, R., Pipunic, R. C., and Sherman, B. S.: Scaling of potential evapotranspiration with MODIS data reproduces flux observations and catchment water balance observations across Australia, J. Hydrol., 369, 107–119, doi:10.1016/j.jhydrol.2009.02.013, 2009. 8, 14

Gumbel, E. J.: Les valeurs extrêmes des distributions statistiques, Annales de l'institut Henri Poincaré, 5, 115–158, 1935. 10, 13

Güntner, A.: Improvement of global hydrological models using GRACE data, Surv. Geophys., 29, 375–397, doi:10.1007/s10712-008-9038-y, 2008. 6

Hagemann, S. and Kleidon, A.: The influence of rooting depth on the simulated hydrological cycle of a GCM, Physics and Chemistry of the Earth, Part B: Hydrology, Ocean. Atmos., 24, 775–779, doi:10.1016/S1464-1909(99)00079-9, 1999. 3

Hallgren, W. S. and Pitman, A. J.: The uncertainty in simulations by a Global Biome Model (BIOME3) to alternative parameter values, Global Change Biol., 6, 483–495, doi:10.1046/j.1365-2486.2000.00325.x, 2000. 3

Hanasaki, N., Kanae, S., Oki, T., Masuda, K., Motoya, K., Shirakawa, N., Shen, Y., and Tanaka, K.: An integrated model for the assessment of global water resources – Part 1: Model description and input meteorological forcing, Hydrol. Earth Syst. Sci., 12, 1007–1025, doi:10.5194/hess-12-1007-2008, 2008. 6

Harris, I., Jones, P., Osborn, T., and Lister, D.: Updated high-resolution grids of monthly climatic observations – the CRU TS3.10 dataset, Int. J. Climatol., 34, 623–642, doi:10.1002/joc.3711, 2014. 14, 16, 26

HESSD

doi:10.5194/hess-2015-533

Global root zone storage capacity

L. Wang-Erlandsson et al.

Discussion Paper | Discussion Paper | Discussion Paper | Discussion Paper

Hildebrandt, A. and Eltahir, E. A. B.: Ecohydrology of a seasonal cloud forest in Dhofar: 2. Role of clouds, soil type, and rooting depth in tree-grass competition, Water Resour. Res., 43, W11411, doi:10.1029/2006WR005262, 2007. 5

Hofste, R., Bastiaanssen, W., Anderson, M., Kustas, W., Hein, C., Seid, A., Senay, G., Verdin, J., van Dijk, A., Guerschman, J., Arancibia, J. L. P., Miralles, D., de Jeu, R., Wada, Y., Menenti, M., and Coenders, A.: Comparative analysis of near-operational evapotranspiration products for the Nile basin based on Earth Observations; First steps towards an ensemble ET product, Master thesis, Delft University of Technology, available at: http://repository.tudelft.nl/assets/uuid:16659a39-3256-4ff9-9930-81ac4dfb4018/maindoc.pdf (last access: 25 December 2015), 2014. 8, 22

Hoogeveen, J., Faurès, J.-M., Peiser, L., Burke, J., and van de Giesen, N.: GlobWat – a global water balance model to assess water use in irrigated agriculture, Hydrol. Earth Syst. Sci., 19, 3829–3844, doi:10.5194/hess-19-3829-2015, 2015. 4

Hu, G. and Jia, L.: Monitoring of evapotranspiration in a semi-arid inland river basin by combining microwave and optical remote sensing observations, Remote Sens., 7, 3056–3087, doi:10.3390/rs70303056, 2015. 8, 24

Hu, G., Jia, L., and Menenti, M.: Comparison of MOD16 and LSA-SAF MSG evapotranspiration products over Europe for 2011, Remote Sens. Environ., 156, 510–526, doi:10.1016/j.rse.2014.10.017, 2015. 22

Hunger, M. and Döll, P.: Value of river discharge data for global-scale hydrological modeling, Hydrol. Earth Syst. Sci., 12, 841–861, doi:10.5194/hess-12-841-2008, 2008. 6

Ichii, K., HASHIMOTO, H., WHITE, M. a., Potter, C., HUTYRA, L. R., HUETE, A. R., Myneni, R. B., and Nemani, R. R.: Constraining rooting depths in tropical rainforests using satellite data and ecosystem modeling for accurate simulation of gross primary production seasonality, Global Change Biol., 13, 67–77, doi:10.1111/j.1365-2486.2006.01277.x, 2007. 6

Ichii, K., Wang, W., Hashimoto, H., Yang, F., Votava, P., Michaelis, A. R., and Nemani, R. R.: Refinement of rooting depths using satellite-based evapotranspiration seasonality for ecosystem modeling in California, Agr. For., 149, 1907–1918, doi:10.1016/j.agrformet.2009.06.019, 2009. 6

Jackson, R. B., Canadell, J., Ehleringer, J. R., Mooney, H. A., Sala, O. E., and Schulze, E. D.: A global analysis of root distributions for terrestrial biomes, Oecologia, 108, 389–411, doi:10.1007/BF00333714, 1996. 4

HESSD

doi:10.5194/hess-2015-533

Global root zone storage capacity

L. Wang-Erlandsson et al.

Jägermeyr, J., Gerten, D., Heinke, J., Schaphoff, S., Kummu, M., and Lucht, W.: Water savings potentials of irrigation systems: global simulation of processes and linkages, Hydrol. Earth Syst. Sci., 19, 3073–3091, doi:10.5194/hess-19-3073-2015, 2015. 14

Jennings, C. M. H. C. M. H.: The hydrology of Botswana, Ph.D. thesis, University of Natal, http://researchspace.ukzn.ac.za/xmlui/handle/10413/8524?show=full (last access: 25 December 2015), 1974. 5

Jhorar, R., van Dam, J., Bastiaanssen, W., and Feddes, R.: Calibration of effective soil hydraulic parameters of heterogeneous soil profiles, J. Hydrol., 285, 233–247, doi:10.1016/j.jhydrol.2003.09.003, 2004. 6

Jolly, W. M., Nemani, R., and Running, S. W.: A generalized, bioclimatic index to predict foliar phenology in response to climate, Global Change Biol., 11, 619–632, doi:10.1111/j.1365-2486.2005.00930.x, 2005. 11

Kleidon, A.: Global datasets of rooting zone depth inferred from inverse methods, J. Clim., 17, 2714–2722, doi:10.1175/1520-0442(2004)017<2714:GDORZD>2.0.CO;2, 2004. 6, 15, 17, 23

Kleidon, A. and Heimann, M.: A method of determining rooting depth from a terrestrial biosphere model and its impacts on the global water and carbon cycle, Global Change Biol., 4, 275–286, doi:10.1046/j.1365-2486.1998.00152.x, 1998a. 6

Kleidon, A. and Heimann, M.: Optimised rooting depth and its impacts on the simulated climate of an atmospheric general circulation model, Geophys. Res. Lett., 25, 345–348, doi:10.1029/98GL00034, 1998b. 3

Kleidon, A. and Heimann, M.: Assessing the role of deep rooted vegetation in the climate system with model simulations: mechanism, comparison to observations and implications for Amazonian deforestation, Clim. Dynam., 16, 183–199, doi:10.1007/s003820050012, 2000. 3

Laio, F., D'Odorico, P., and Ridolfi, L.: An analytical model to relate the vertical root distribution to climate and soil properties, Geophys. Res. Lett., 33, L18401, doi:10.1029/2006GL027331, 2006. 5

Lee, J.-E., Oliveira, R. S., Dawson, T. E., and Fung, I.: Root functioning modifies seasonal climate., P. Natl. Acad. Sci. USA, 102, 17576–17581, doi:10.1073/pnas.0508785102, 2005. 3

Matsumoto, K., Ohta, T., Nakai, T., Kuwada, T., Daikoku, K., Iida, S., Yabuki, H., Kononov, A. V., van der Molen, M. K., Kodama, Y., Maximov, T. C., Dolman, A. J., and Hattori, S.: Responses

HESSD

doi:10.5194/hess-2015-533

Global root zone storage capacity

L. Wang-Erlandsson et al.

of surface conductance to forest environments in the Far East, Agr. For. Meteorol., 148, 1926–1940, doi:10.1016/j.agrformet.2008.09.009, 2008. 12

Milly, P. C. D.: Climate, soil water storage, and the average annual water balance, Water Resour. Res., 30, 2143–2156, doi:10.1029/94WR00586, 1994. 3, 7

5 Milly, P. C. D. and Dunne, K. A.: Sensitivity of the global water cycle to the water-holding capacity of land, J. Clim., 7, 506–526, doi:10.1175/1520-0442(1994)007<0506:SOTGWC>2.0.CO;2, 1994. 3, 7

Monteith, J. L.: Evaporation and environment, in: Symp Soc Exp Biol, vol. 19, chap. The State, 205–234, Cambridge University Press, Swansea, 1965. 11

10 Mu, Q., Zhao, M., and Running, S. W.: Improvements to a MODIS global terrestrial evapotranspiration algorithm, Remote Sens. Environ., 115, 1781–1800, doi:10.1016/j.rse.2011.02.019, 2011. 8, 14

Müller Schmied, H., Eisner, S., Franz, D., Wattenbach, M., Portmann, F. T., Flörke, M., and Döll, P.: Sensitivity of simulated global-scale freshwater fluxes and storages to input data, 15 hydrological model structure, human water use and calibration, Hydrol. Earth Syst. Sci., 18, 3511–3538, doi:10.5194/hess-18-3511-2014, 2014. 5

Nepstad, D. C., de Carvalho, C. R., Davidson, E. A., Jipp, P. H., Lefebvre, P. A., Negreiros, G. H., da Silva, E. D., Stone, T. A., Trumbore, S. E., and Vieira, S.: The role of deep roots in the hydrological and carbon cycles of Amazonian forests and pastures, Nature, 372, 666–669, 20 doi:10.1038/372666a0, 1994. 5

Nijssen, B., O'Donnell, G. M., Lettenmaier, D. P., Lohmann, D., and Wood, E. F.: Predicting the discharge of global rivers, J. Clim., 14, 3307–3323, doi:10.1175/1520-0442(2001)014<3307:PTDOGR>2.0.CO;2, 2001. 6

Phillips, W. S.: Depth of roots in Soil, Ecology, 44, 424, doi:10.2307/1932198, 1963. 5

25 Saxton, K. E. and Rawls, W. J.: Soil water characteristic estimates by texture and organic matter for hydrologic solutions, Soil Sci. Soc. Am. J., 70, 1569, doi:10.2136/sssaj2005.0117, 2006. 16

Schenk, H. and Jackson, R.: The global biogeography of roots, Ecol. Monogr., 72, 311–328, doi:10.1890/0012-9615(2002)072[0311:TGBOR]2.0.CO;2, 2002. 4

30 Schenk, H. J.: The shallowest possible water extraction profile: a null model for global root distributions, Vadose Zone J., 7, 1119, doi:10.2136/vzj2007.0119, 2008. 5, 6, 7, 21

Schenk, H. J. and Jackson, R. B.: ISLSCP II Ecosystem rooting depths, in: ISLSCP Initiative II Collection, edited by G., F., Collatz, G., Meeson, B., Los, S., de Colstoun, E. B., and Landis,

Discussion Paper | Discussion Paper | Discussion Paper | Discussion Paper | Discussion Paper |

HESSD

doi:10.5194/hess-2015-533

Global root zone storage capacity

L. Wang-Erlandsson et al.

D., Oak Ridge National Laboratory Distributed Active Archive Center, Oak Ridge, Tennessee, USA, doi:10.3334/ORNLDAAC/929, http://daac.ornl.gov/ (last access: 6 September 2015), 2009. 4, 15, 17, 21, 23

Schneider, U., Becker, A., Finger, P., Meyer-Christoffer, Anja Rudolf, B., and Ziese, M.: GPCC full data reanalysis version 6.0 at 0.5: Monthly land-surface precipitation from rain-gauges built on GTS-based and historic data, doi:10.5676/DWD_GPCC/FD_M_V6_050, 2011. 27

Schwinning, S. and Ehleringer, J. R.: Water use trade-offs and optimal adaptations to pulse-driven arid ecosystems, J. Ecology, 89, 464–480, doi:10.1046/j.1365-2745.2001.00576.x, 2001. 5

Senay, G. B., Bohms, S., Singh, R. K., Gowda, P. H., Velpuri, N. M., Alemu, H., and Verdin, J. P.: Operational evapotranspiration mapping using remote sensing and weather datasets: A new parameterization for the SSEB approach, J. Am. Water Resour. Assoc., 49, 577–591, doi:10.1111/jawr.12057, 2013. 14

Sivandran, G. and Bras, R. L.: Dynamic root distributions in ecohydrological modeling: A case study at Walnut Gulch Experimental Watershed, Water Resour. Res., 49, 3292–3305, doi:10.1002/wrcr.20245, 2013. 4

Smithwick, E. A., Lucash, M. S., McCormack, M. L., and Sivandran, G.: Improving the representation of roots in terrestrial models, Ecol. Model., 291, 193–204, doi:10.1016/j.ecolmodel.2014.07.023, 2014. 6

Stewart, J.: Modelling surface conductance of pine forest, Agr. For. Meteorol., 43, 19–35, doi:10.1016/0168-1923(88)90003-2, 1988. 11

Stone, E. and Kalisz, P.: On the maximum extent of tree roots, Forest Ecol. Manage., 46, 59–102, doi:10.1016/0378-1127(91)90245-Q, 1991. 5

Trambauer, P., Dutra, E., Maskey, S., Werner, M., Pappenberger, F., van Beek, L. P. H., and Uhlenbrook, S.: Comparison of different evaporation estimates over the African continent, Hydrol. Earth Syst. Sci., 18, 193–212, doi:10.5194/hess-18-193-2014, 2014. 22

van Dijk, A., Warren, G., Van Niel, T., Byrne, G., Pollock, D., and Doody, T.: Derivation of data layers from medium resolution remote sensing to support mapping of groundwater dependent ecosystems, Tech. rep., A report for the National Water Commission, 27 pp., 2014. 7, 8, 22, 24

van Wijk, M. T. and Bouten, W.: Towards understanding tree root profiles: simulating hydrologically optimal strategies for root distribution, Hydrol. Earth Syst. Sci., 5, 629–644, doi:10.5194/hess-5-629-2001, 2001. 5

HESSD

doi:10.5194/hess-2015-533

Global root zone storage capacity

L. Wang-Erlandsson et al.

Wang-Erlandsson, L., van der Ent, R. J., Gordon, L. J., and Savenije, H. H. G.: Contrasting roles of interception and transpiration in the hydrological cycle – Part 1: Temporal characteristics over land, Earth Syst. Dynam., 5, 441–469, doi:10.5194/esd-5-441-2014, 2014. 5, 11, 12, 15, 18

Werth, S. and Güntner, A.: Calibration analysis for water storage variability of the global hydrological model WGHM, Hydrol. Earth Syst. Sci., 14, 59–78, doi:10.5194/hess-14-59-2010, 2010. 6

Widén-Nilsson, E., Halldin, S., and Xu, C.-y.: Global water-balance modelling with WASMOD-M: Parameter estimation and regionalisation, J. Hydrol., 340, 105–118, doi:10.1016/j.jhydrol.2007.04.002, 2007. 6

Winsemius, H. C., Schaefli, B., Montanari, A., and Savenije, H. H. G.: On the calibration of hydrological models in ungauged basins: A framework for integrating hard and soft hydrological information, Water Resour. Res., 45, W12422, doi:10.1029/2009WR007706, 2009. 6

Yilmaz, M. T., Anderson, M. C., Zaitchik, B., Hain, C. R., Crow, W. T., Ozdogan, M., Chun, J. A., and Evans, J.: Comparison of prognostic and diagnostic surface flux modeling approaches over the Nile River basin, Water Resour. Res., 50, 386–408, doi:10.1002/2013WR014194, 2014. 22

Zeng, X.: Global vegetation root distribution for land modeling, J. Hydrometeorol., 2, 525–530, doi:10.1175/1525-7541(2001)002<0525:GVRDFL>2.0.CO;2, 2001. 4, 5

Zeng, X., Dai, Y.-J., Dickinson, R. E., and Shaikh, M.: The role of root distribution for climate simulation over land, Geophys. Res. Lett., 25, 4533–4536, doi:10.1029/1998GL900216, 1998. 4

HESSD

doi:10.5194/hess-2015-533

Global root zone storage capacity

L. Wang-Erlandsson et al.

Discussion Paper | Discussion Paper | Discussion Paper | Discussion Paper | Discussion Paper |

HESSD

doi:10.5194/hess-2015-533

Global root zone storage capacity

L. Wang-Erlandsson et al.

Table 1. Overview of the time period, latitudinal coverage and data input for the two S_R datasets ($S_{R,\text{CHIRPS-CSM}}$ and $S_{R,\text{CRU-SM}}$) produced in this study.

	$S_{R,\text{CHIRPS-CSM}}$	$S_{R,\text{CRU-SM}}$
Years	2003–2012	2003–2013
Latitude coverage	50° N–50° S	80° N–56° S
Monthly P data input	CHIRPS	CRU
Monthly E data input	Mean of CMRSET, SSEBop, and MOD16 (E_{CSM})	Mean of SSEBop and MOD16 (E_{SM})
Monthly irrigation data input	LPJmL (2003–2009)	LPJmL (2003–2009)
Daily E and P data for downscaling	ERA-I	ERA-I

Discussion Paper | Discussion Paper | Discussion Paper | Discussion Paper | Discussion Paper |

HESSD

doi:10.5194/hess-2015-533

Global root zone storage capacity

L. Wang-Erlandsson et al.

Table B1. Predictor variables selected by AIC for the different land cover types.

Land cover type	Predictor variables
02:evergreen needleleaf forest	$S_R = I_{isd} + I_s + I_a + I_{isd}{:}I_a + I_s{:}I_a$
03:evergreen broadleaf forest	$S_R = I_{isd} + I_s + I_a + I_{isd}{:}I_s + I_s{:}I_a$
04:deciduous needleleaf forest	$S_R = I_{isd} + I_s + I_a + I_s{:}I_a + I_{isd}{:}I_a + I_{isd}{:}I_s + I_{isd}{:}\,I_s{:}I_a$
05:deciduous broadleaf forest	$S_R = I_{isd} + I_s + I_a + I_s{:}I_a + I_{isd}{:}I_s$
06:mixed forests	$S_R = I_{isd} + I_s + I_a + I_{isd}{:}I_a + I_{isd}{:}I_s + I_s{:}I_a + I_{isd}{:}I_s{:}I_a$
08:open shrublands	$S_R = I_{isd} + I_s + I_a + I_{isd}{:}I_a + I_{isd}{:}I_s + I_s{:}I_a + I_{isd}{:}I_s{:}I_a$
09:woody savannas	$S_R = I_{isd} + I_s + I_a + I_{isd}{:}I_a + I_s{:}I_a$
10:savannas	$S_R = I_{isd} + I_s + I_a + I_{isd}{:}I_a + I_s{:}I_a + I_{isd}{:}I_s + I_{isd}{:}I_s{:}I_a$
11:grasslands	$S_R = I_{isd} + I_s + I_a + I_{isd}{:}I_s + I_s{:}I_a$
13:croplands	$S_R = I_{isd} + I_s + I_a + I_{isd}{:}I_a + I_{isd}{:}I_s + I_s{:}I_a + I_{isd}{:}\,I_s{:}I_a$
15:cropland/natural veg. mosaic	$S_R = I_{isd} + I_s + I_a + I_{isd}{:}I_s$
17:barren or sparsely vegetated	$S_R = I_{isd} + I_s + I_a + I_s{:}I_a + I_{isd}{:}\,I_a + I_{isd}{:}I_s$

HESSD

doi:10.5194/hess-2015-533

Global root zone storage capacity

L. Wang-Erlandsson et al.
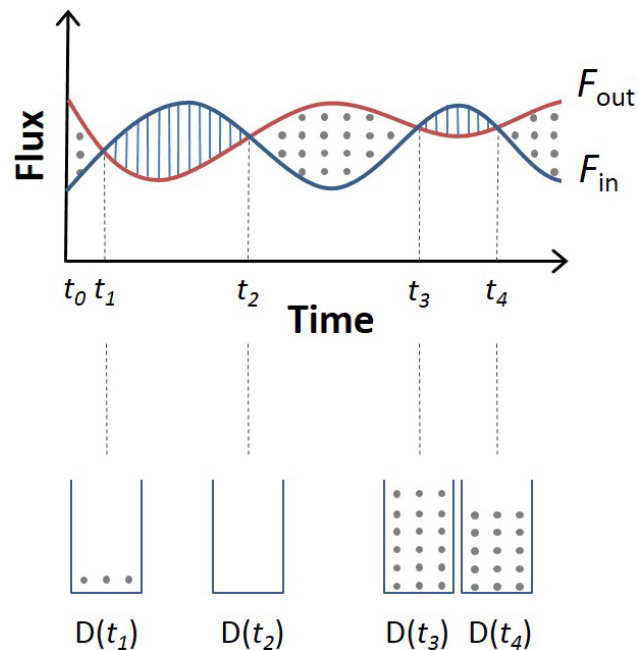
Figure 1. Conceptual illustration of the algorithm for calculating the root zone storage capacity S_R. The shaded areas represent the accumulated differences A that are positive when outflow $F_{out} > $ inflow F_{in}, and negative when $F_{out} < F_{in}$. Moisture deficit D is increased by positive A and decreased by negative A. Note that D never becomes negative in order to take surface runoff into account.

PRECIPITATION DATA

Mean annual P_{CHIRPS}, 2003–2012
(a)

Mean annual P_{CRU}, 2003–2013
(b)

EVAPORATION DATA

Mean annual E_{CSM}, 2003–2012
(c)

Mean annual E_{SM}, 2003–2013
(d)

Standard deviation of E_{CSM}, 2003–2012
(e)

Standard deviation of E_{SM}, 2003–2013
(f)
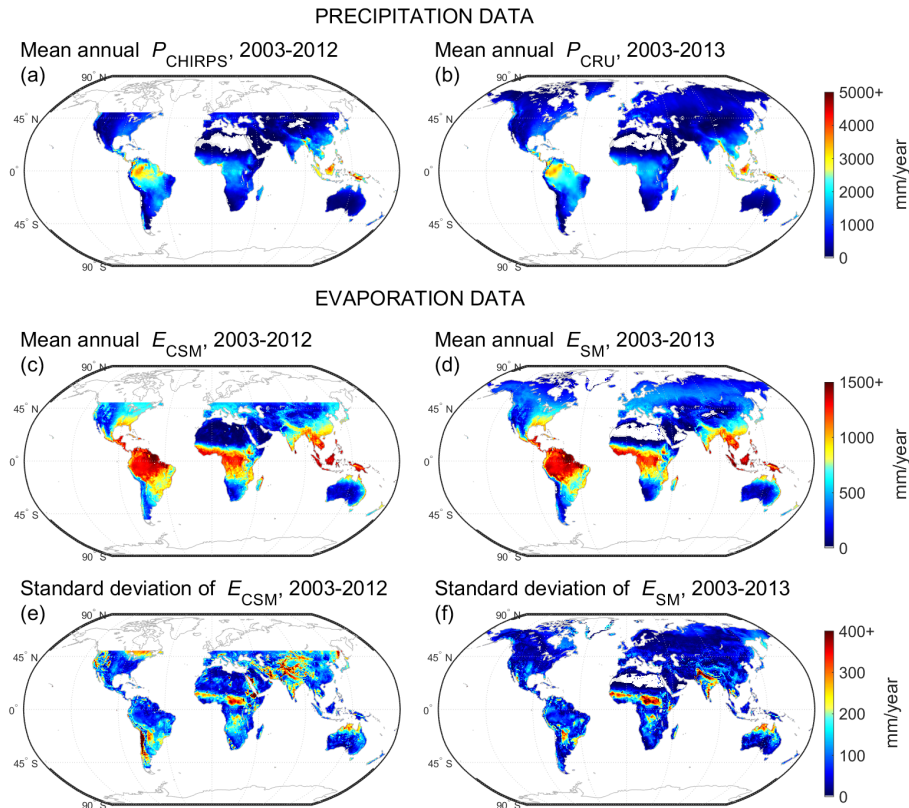
Figure 2. The mean annual precipitation of **(a)** CHIRPS for the years 2003–2012 (50° N–50° S), and **(b)** CRU for the years 2003–2013 (80° N–56° S). The mean annual ensemble evaporation of **(c)** CMRSET, SSEBop and MOD16 for the years 2003–2012 (50° N–50° S), and **(e)** SSEBop and MOD16 for the years 2003–2013 (80° N–56° S). Standard deviation of ensemble evaporation of **(e)** CMRSET, SSEBop and MOD16 for the years 2003–2012 (50° N–50° S), and **(f)** SSEBop and MOD16 for the years 2003–2013 (80° N–56° S).

Discussion Paper | Discussion Paper | Discussion Paper | Discussion Paper |

HESSD

doi:10.5194/hess-2015-533

Global root zone storage capacity

L. Wang-Erlandsson et al.

HESSD

doi:10.5194/hess-2015-533

**Global root zone
storage capacity**

L. Wang-Erlandsson et
al.
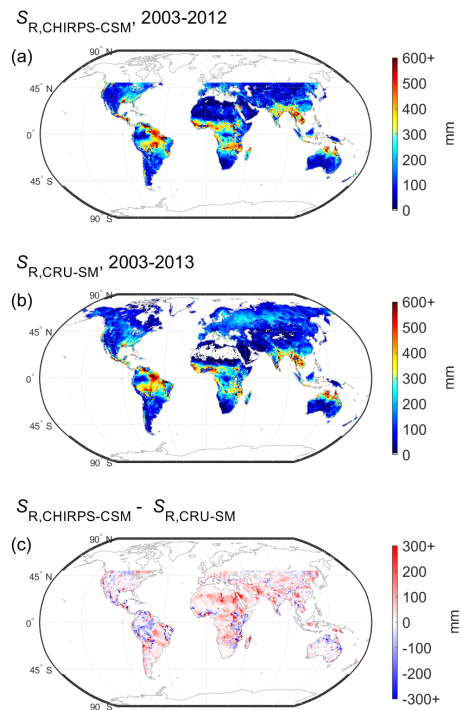
Figure 3. (a) $S_{R,CHIRPS-CSM}$, **(b)** $S_{R,CRU-SM}$, and **(c)** the difference between $S_{R,CHIRPS-CSM}$ and $S_{R,CRU-SM}$.

Full Screen / Esc

Discussion Paper | Discussion Paper | Discussion Paper | Discussion Paper |

HESSD

doi:10.5194/hess-2015-533

Global root zone storage capacity

L. Wang-Erlandsson et al.
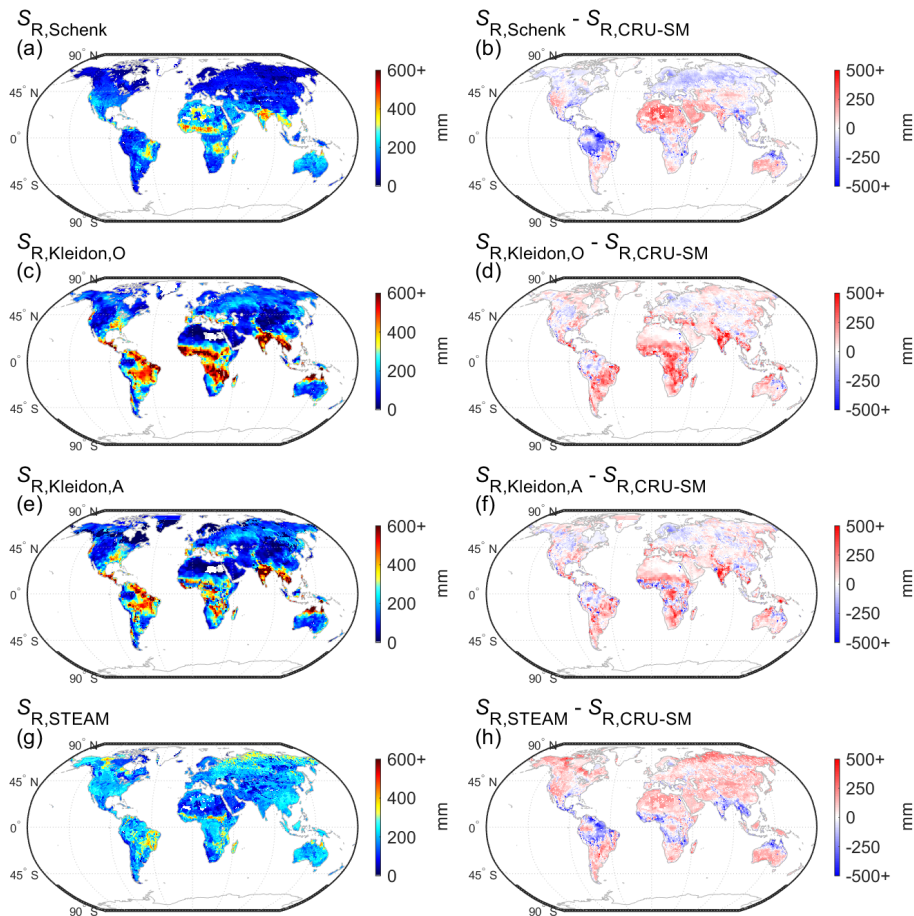
Figure 4. Root zone storage capacities of **(a)** $S_{R,Schenk}$, **(c)** $S_{R,Kleidon,O}$, **(e)** $S_{R,Kleidon,A}$, **(g)** $S_{R,STEAM}$ and **(b, d, f, h)** their differences with $S_{R,CRU-SM}$.

HESSD

doi:10.5194/hess-2015-533

Global root zone storage capacity

L. Wang-Erlandsson et al.
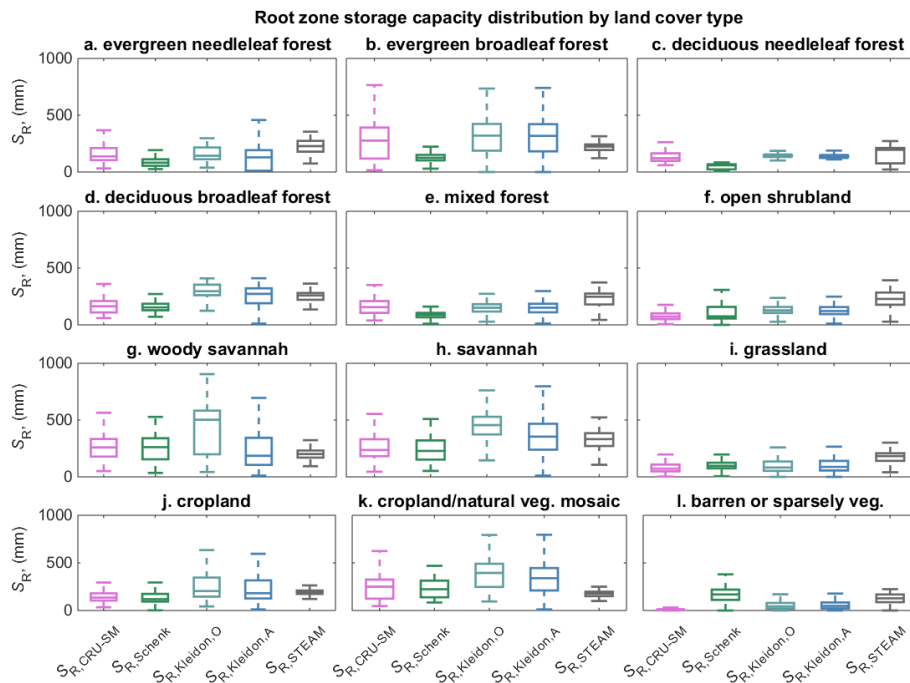
Figure 5. Comparison of root zone storage capacity estimates by land cover type using Tukey boxplots. The central markers of the boxes mark the median, and the box edges mark the 25th and 75th percentile. The whiskers extend to 1.5 times the interquartile range.

HESSD

doi:10.5194/hess-2015-533

Global root zone storage capacity

L. Wang-Erlandsson et al.
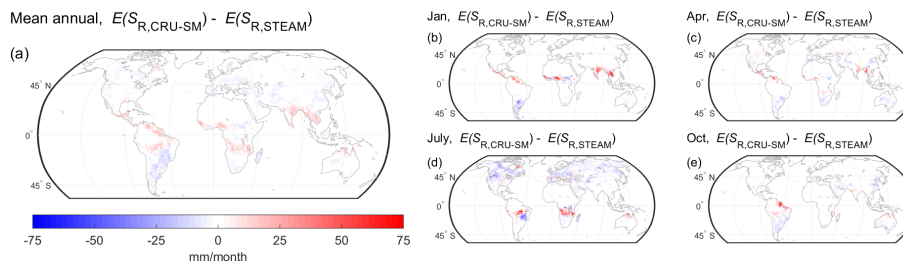
Figure 6. Difference in STEAM-simulated evaporation between using $S_{R,CRU-SM}$ and $S_{R,STEAM}$ as root zone storage capacity parametrisation at **(a)** mean annual scale and averages for the months of **(b)** January, **(c)** April, **(d)** July, and **(e)** October over the time period 2003–2013. See also Sect. 4.3.
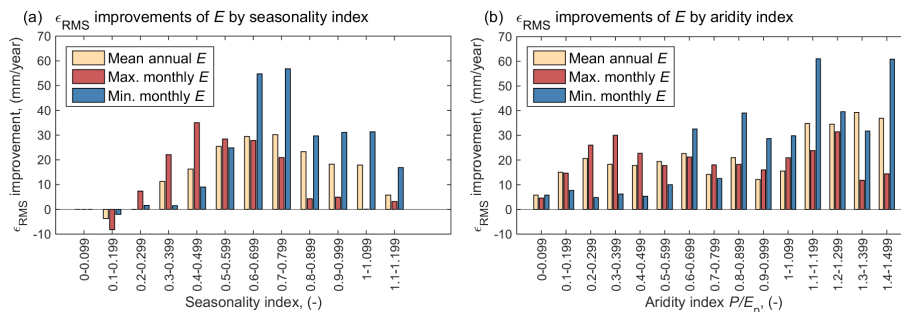
Figure 7. The ε_{RMS} improvement in simulated mean monthly E by implementing $S_{R,CRU-SM}$ instead $S_{R,STEAM}$ in STEAM. The improvements in mean annual, mean maximum monthly and mean minimum monthly E (over the years 2003–2013) are sorted by **(a)** precipitation seasonality index and **(b)** aridity index. The satellite based E_{SM} was used as the benchmark for improvements.

HESSD

doi:10.5194/hess-2015-533

Global root zone storage capacity

L. Wang-Erlandsson et al.

Discussion Paper | Discussion Paper | Discussion Paper | Discussion Paper | Discussion Paper |

HESSD

doi:10.5194/hess-2015-533

Global root zone storage capacity

L. Wang-Erlandsson et al.

Figure 8. Mean latitudinal **(a)** $S_{R,CHIRPS-CSM}$ and **(b)** $S_{R,CRU-SM}$ dimensioned by drought return periods between 2 and 60 years estimated using Gumbel distribution.
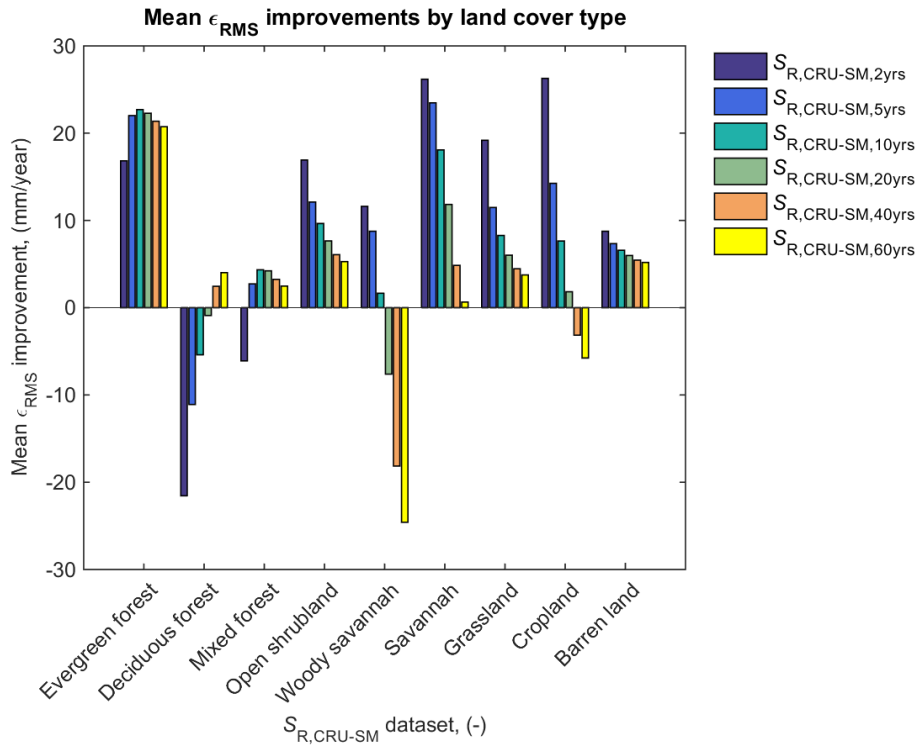
Figure 9. The mean ε_{RMS} improvement in simulated monthly E (2003–2013) by implementing $S_{R,CRU-SM,Lyrs}$ instead of $S_{R,STEAM}$ in STEAM, where the satellite based E_{SM} was used as the benchmark for improvements. The improvements for $S_{R,CRU-SM,2yrs}$, $S_{R,CRU-SM,5yrs}$, $S_{R,CRU-SM,10yrs}$, $S_{R,CRU-SM,20yrs}$, $S_{R,CRU-SM,40yrs}$, and $S_{R,CRU-SM,60yrs}$ are shown for the different land cover types that has >90 % grid cell coverage. Land cover types represented in less than 50 grid cells are lumped together: evergreen forest (needleleaf and broadleaf); deciduous forest (needleleaf and broadleaf); and cropland (cropland and cropland/natural vegetation mosaic).

HESSD

doi:10.5194/hess-2015-533

Global root zone storage capacity

L. Wang-Erlandsson et al.

Discussion Paper | Discussion Paper | Discussion Paper | Discussion Paper | Discussion Paper |

HESSD

doi:10.5194/hess-2015-533

Global root zone storage capacity

L. Wang-Erlandsson et al.

Mean annual exceedance of E_{CSM} over P_{CHIRPS}, 2003-2012

Mean annual exceedance of E_{SM} over P_{CRU}, 2003-2013
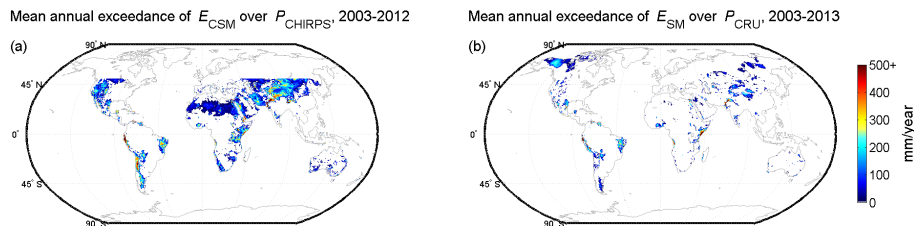
Figure A1. Mean annual accumulated exceedance of **(a)** E_{CSM} over P_{CHIRPS}, and **(b)** E_{SM} over P_{CRU}.

Discussion Paper | Discussion Paper | Discussion Paper | Discussion Paper

HESSD

doi:10.5194/hess-2015-533

Global root zone storage capacity

L. Wang-Erlandsson et al.
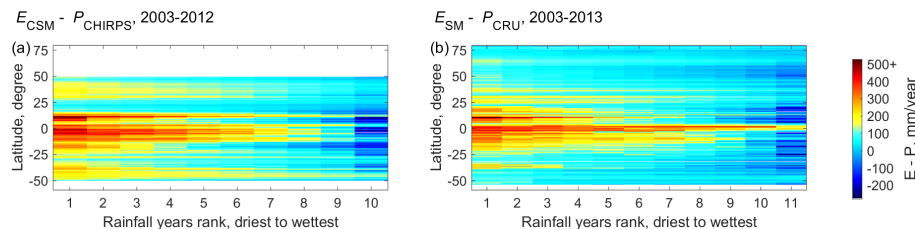
Figure A2. Mean latitudinal difference between **(a)** E_{CSM} and P_{CHIRPS}, and **(b)** E_{SM} and P_{CRU} sorted from the driest to the wettest years. The figure only includes regions where accumulated $E - P$ over the entire available time series (2003–2012 and 2003–2013 respectively) are positive.
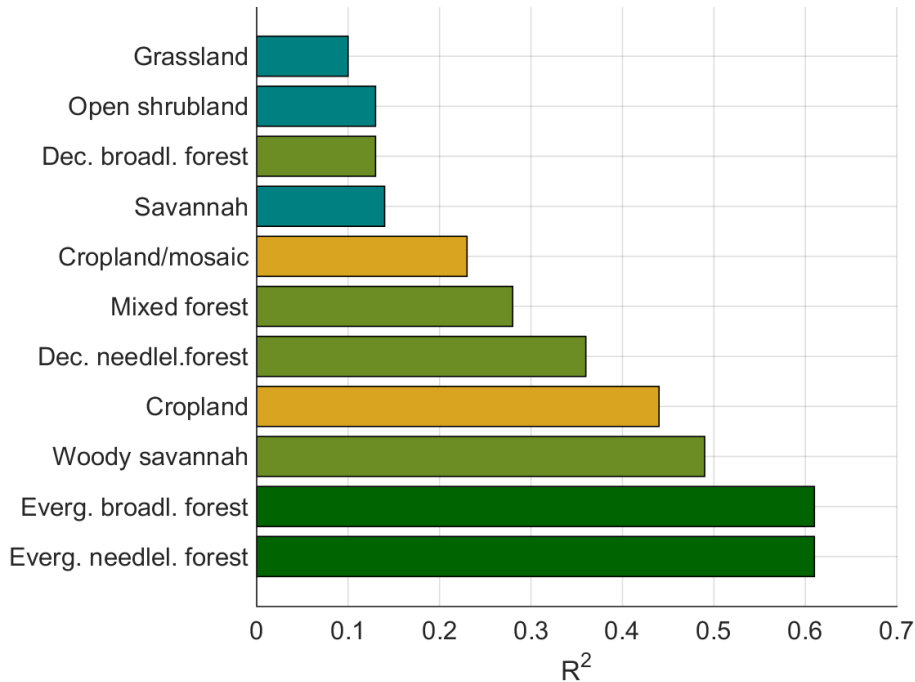
Figure B1. R^2 of the multiple linear regression model of $S_{R,CRU-SM}$ based on the climate variables interstorm duration I_{isd}, precipitation seasonality I_s, and aridity I_a. The green bars are forests or wooded land, the yellow bars represent croplands, and the teal bars represent short vegetation types.

HESSD

doi:10.5194/hess-2015-533

Global root zone storage capacity

L. Wang-Erlandsson et al.